

## A review on the numerical simulation model of scouring around bridge pier by using Flow-3D software

Aisyah Dwi Puspasari<sup>1</sup> and Jyh Haw-Tang<sup>2</sup>

<sup>1</sup>Department of Civil Engineering, Faculty of Civil Engineering and Planning, Institut Teknologi Adhi Tama Surabaya

<sup>2</sup>Department of Civil Engineering, Chung Yuan Christian University

**Abstract.** Scouring is a critical issue that can lead to structural damage. Local scour, in particular, has motivated extensive research to understand its causes and to predict the maximum scouring depth around the bridge pier. Numerical simulation, particularly using Flow-3D software, has emerged as an effective tool for predicting and monitoring scour depth, ensuring the stability and safety of bridges. Flow-3D is an accurate, fast, proven CFD software is capable of addressing complex free-surface flow challenges. However, detailed guidelines for its use are limited. The review highlights the importance of scour prediction, discusses scour mechanisms, evaluates turbulence models, and compares numerical and experimental results to determine the most accurate model. The paper also discusses the Flow-3D model setup, including governing equations, sediment scour models, meshing techniques, and boundary conditions. The Renormalized Group (RNG)  $k-\epsilon$  turbulence model and Soulsby-Whitehouse and Van Rijn sediment transport equations are identified as the most effective for simulating scour. Zhang's study is highlighted as the most accurate numerical model, with a 0% error rate compared to experimental results. The left and right boundaries were defined by specified velocity and outflow, while symmetry was applied to the front and back boundaries. The bottom and top boundaries were modeled as walls and specified pressure, respectively. The paper concludes with recommendations for future research, including the integration of real-time scour monitoring and machine learning in CFD modeling.

**Keywords:** Scouring, bridge pier, numerical modeling, Flow-3D, verification

### 1. Introduction

Scour occurs naturally as a result of flowing water in rivers (Breusers, 1979; Ghasemi and Soltani-Gerdefaramarzi, 2017) and streams, primarily linked to changes in the riverbed through processes of aggradation and degradation (Wang, Liang and Yu, 2016; Ghasemi and Soltani-Gerdefaramarzi, 2017). Water flow erodes the bed particles and transports them past obstructions (Breusers, Nicollet and Shen, 1977; Ghaderi and Abbasi, 2019), driven by factors such as acceleration of flow, turbulence, and the erosive characteristics of the moving water (Briaud, Gardoni and Yao, 2012; Soltani-Gerdefaramarzi, Afzalimehr, Yee-Meng Chiew, *et al.*, 2013).

Three primary types of scouring are identified: general scour, contraction scour, and local scour (Prendergast and Gavin, 2014). In river channels, general scouring occurs naturally due to the processes of aggradation and degradation that affect the riverbed. A significant change in the hydraulic conditions of the river is considered the primary reason for this scouring type. Contraction scour occurs when the width of a channel is narrowed, particularly around bridge piers or abutments, which results in an increase in flow velocity and shear stress on the bed, facilitating sediment movement (Briaud, Gardoni and Yao, 2012). Local scour, the focus of this paper, occurs near bridge piers or abutments, where downward flow at the upstream end of the pier causes localized erosion, removing sediment from the base of the structure as shown in **Figure 1**. It relies on the equilibrium between streambed erosion and sediment deposition (Soltani-Gerdefaramarzi, Afzalimehr, Chiew, *et al.*, 2013; Prendergast and Gavin, 2014). Local scour can be divided into two categories: clear water scour and live bed scour. In clear water scour, there is no sediment supplied by the river's approaching flow, whereas an interaction occurs between sediment transport and the live bed scour stage (Ghasemi and Soltani-Gerdefaramarzi, 2017).

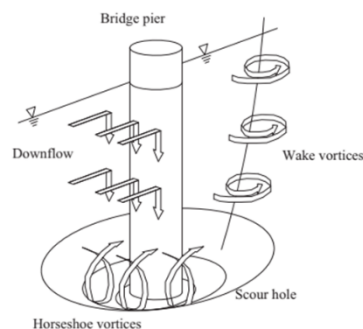


**Figure 1.** Schematic of the scouring process (Hamill, 1999)

In the construction of dams, reservoirs, piping systems, settling ponds, flood management systems, sediment scouring, and deposition is an important factor (Brethour, 2001), likewise for the bridge pier. Scouring occurs locally around separate bridge piers and abutments and is widely recognized as a primary reason for bridge failures because of the increasing scouring depth, then the bridge pier may become unstable and collapse, causing major human and financial losses (Hamill, 1999; Ghasemi and Soltani-Gerdefaramarzi, 2017). (Richardson and Panchang, 1998) define the scouring mechanism as the mean flow in the center hits the pier, it is forced to separate and flow around the pier. A part of the approaching flow was also observed to pass down the obstacle's upstream face. The relation between this downward flow and the flow of the horizontal boundary layer close to the channel bed leads to the formation of a horseshoe vortex at the pier's foundation. This vortex, characterized by a horizontal axis of rotation, has a significant influence on the scouring action at the saddle's base. Based on the adverse impact of scouring, it is important to monitor the depth of scouring to manage the stability and safety of the bridge (Prendergast and Gavin, 2014; Alemi and Maia, 2016) and avoid the damages that may occur (Ghasemi and Soltani-Gerdefaramarzi, 2017). This review provides comprehensive information on sediment scour modeling utilizing Flow-3D software to determine the most accurate numerical model.

## 2. Numerical simulation

### 2.1 Computational fluid dynamics (CFD)

Computational Fluid Dynamics, often referred to as CFD, entails the simulation of fluid movement through the process of breaking down and resolving conventional flow equations, including the Navier-Stokes equations and continuity equations, for individual computational cells (Flow Science, 2008). CFD has emerged as a powerful tool for modeling and simulating complex hydraulic problems (Wang, Liang and Yu, 2016). Through numerical simulations, intricate models that are challenging to replicate in laboratory settings can be easily analyzed (Jalal and Hassan, 2020). CFD analysis, performed using advanced computers, provides detailed insights into flow velocity fields, bed shear stress, and scour depth, surpassing the capabilities of physical models (Alemi and Maia, 2016). For accurate results, the numerical model must closely represent the real-life situation accurately, and key parameters must be carefully selected. Moreover, the problem being modeled should reflect as closely as possible the real physical situation. Several popular CFD software including ANSYS, OpenFOAM, PowerFLOW, SimScale, COMSOL, Flow-3D, are available, with Flow-3D being the focus of this study.

### 2.2 Flow-3D

Flow-3D represents a commercial computational fluid dynamics (CFD) software that includes specific modules tailored for hydraulic engineering applications. It employs advanced computational methods to resolve equations pertaining to fluid motion, offering transient, three-dimensional solutions to complex, multi-faceted flow challenges. With a variety of both physical and numerical options, Flow-3D accommodates a diverse array of fluid flow situations and heat transfer phenomena. This software is extensively utilized for tackling an assortment of hydraulic issues (Flow Science, 2008) capable of handling highly intricate geometries and physical scenarios. Developed by Flow Science Inc., the FLOW-3D CFD tool utilizes two techniques, VOF and FAVOR, to ascertain the positions of free surfaces and obstacles. Flow-3D effectively simulates the scouring effects surrounding bridge piers and demonstrates proficiency in analyzing the dynamics of specialized liquids and gases, particularly for addressing transient, free-surface, and sediment transport challenges. The solution of the Navier-Stokes equations in three dimensions is accomplished through the implementation of a non-hydrostatic finite difference model (Jalal and Hassan, 2020).

#### 2.2.1 Governing equations

The equations known as Reynolds-Averaged Navier-Stokes, commonly referred to as RANS equations, serve as the primary equations governing the incompressible motion of viscous fluids surrounding bridge pile foundations. All equations incorporate area fractions  $A_i$  and volume fractions  $V_F$ . The continuity equation is expressed as follows:

$$\frac{\partial \langle u_i A_i \rangle}{\partial x_i} = 0 \quad (1)$$

Subsequently, by incorporating extra variables into the  $x$ ,  $y$ , and  $z$  coordinates, the equations governing the motion for the fluid velocity components ( $u$ ,  $v$ , and  $w$ ) can be expressed in the following manner:

$$\begin{aligned}\frac{\partial u}{\partial t} + \frac{1}{V_F} \left( uA_x \frac{\partial u}{\partial x} + vA_y \frac{\partial u}{\partial y} + wA_z \frac{\partial u}{\partial z} \right) &= -\frac{1}{\rho} \frac{\partial p}{\partial x} + G_x + f_x \\ \frac{\partial v}{\partial t} + \frac{1}{V_F} \left( uA_x \frac{\partial v}{\partial x} + vA_y \frac{\partial v}{\partial y} + wA_z \frac{\partial v}{\partial z} \right) &= -\frac{1}{\rho} \frac{\partial p}{\partial y} + G_y + f_y \\ \frac{\partial w}{\partial t} + \frac{1}{V_F} \left( uA_x \frac{\partial w}{\partial x} + vA_y \frac{\partial w}{\partial y} + wA_z \frac{\partial w}{\partial z} \right) &= -\frac{1}{\rho} \frac{\partial p}{\partial z} + G_z + f_z\end{aligned}\quad (2)$$

Where  $x_i$  represents the Cartesian coordinate,  $A_i$  denotes the area fraction,  $V_F$  signifies the volume fraction,  $u_i$  indicates the velocity,  $\rho$  refers to the fluid density,  $p$  is the average hydrodynamic pressure,  $G_i$  stands for the body acceleration, and  $f_i$  is the viscous acceleration ( $i = x, y, z$ ). The expressions for viscous accelerations can be formulated as follows:

$$\begin{aligned}\rho V_F f_x &= -\left[ \frac{\partial}{\partial x} (A_x \tau_{xx}) + \frac{\partial}{\partial y} (A_y \tau_{yx}) + \frac{\partial}{\partial z} (A_z \tau_{zx}) \right] \\ \rho V_F f_y &= -\left[ \frac{\partial}{\partial x} (A_x \tau_{xy}) + \frac{\partial}{\partial y} (A_y \tau_{yy}) + \frac{\partial}{\partial z} (A_z \tau_{zy}) \right] \\ \rho V_F f_z &= -\left[ \frac{\partial}{\partial x} (A_x \tau_{xz}) + \frac{\partial}{\partial y} (A_y \tau_{yz}) + \frac{\partial}{\partial z} (A_z \tau_{zz}) \right]\end{aligned}\quad (3)$$

In which the shear stress  $\tau_{ij}$  ( $i, j = x, y, z$ ) are present:

$$\begin{aligned}\tau_{xx} &= -2\mu \left[ \frac{\partial u}{\partial x} - \frac{1}{3} \left( \frac{\partial u}{\partial x} + \frac{\partial v}{\partial y} + \frac{\partial w}{\partial z} \right) \right] \\ \tau_{yy} &= -2\mu \left[ \frac{\partial v}{\partial y} - \frac{1}{3} \left( \frac{\partial u}{\partial x} + \frac{\partial v}{\partial y} + \frac{\partial w}{\partial z} \right) \right] \\ \tau_{zz} &= -2\mu \left[ \frac{\partial w}{\partial z} - \frac{1}{3} \left( \frac{\partial u}{\partial x} + \frac{\partial v}{\partial y} + \frac{\partial w}{\partial z} \right) \right] \\ \tau_{xy} = \tau_{yx} &= -\mu \left( \frac{\partial u}{\partial x} + \frac{\partial v}{\partial y} \right) \\ \tau_{xz} = \tau_{zx} &= -\mu \left( \frac{\partial u}{\partial x} + \frac{\partial w}{\partial z} \right) \\ \tau_{zy} = \tau_{yz} &= -\mu \left( \frac{\partial w}{\partial z} + \frac{\partial v}{\partial y} \right)\end{aligned}\quad (4)$$

where  $\mu$  is the dynamic viscosity.

### 2.2.2 Turbulence model

Turbulence, when there are inadequate stabilizing forces, is the erratic, unpredictable movement of fluids (i.e., insufficient viscosity). The natural instability that exists within the flow does not dampen out at high Reynolds numbers, resulting in the development of eddies of different lengths. The activity is easily identifiable by the striations apparent on the exposed surface when water flows from the faucet or during the rapid movement of a stream (Flow Science, 2008). For additional nonlinear Reynolds stress term modeling, a turbulence model is required (Ghaderi and Abbasi, 2019). Withing Flow-3D software, users have access to six distinct turbulence model: the Prandtl mixing length model, the one-equation model,

the two-equation ( $k-\varepsilon$ ) model, renormalized group (RNG) model, two-equation ( $k-\omega$ ) model and the large eddy simulation (LES) model.

The Prandtl mixing length model represents the most basic approach, presuming that in regions of high shear, the processes of turbulent mixing occur, such as near solid boundaries, increase fluid viscosity. This is only sufficient, however, for completely established, close to steady flows. This model assumes the development and dissipation of turbulence are in balance anywhere in the flow. This indicates that factors such as turbulent energy advection, diffusion, and the rate of change over time are not taken into account. Due to its limiting assumptions, this model is not as advantageous as the one-equation and two-equation turbulence transport models. The one-equation turbulence transport model, which represents the specific kinetic energy linked to turbulent fluctuations in the flow rate, is known as the turbulent kinetic energy. The model additionally needs the generation of turbulent kinetic energy, which arises from shearing and buoyancy, along with diffusion and dissipation caused by viscous losses within turbulent eddies. The growth of buoyancy occurs solely in the presence of a density gradient in the flow, incorporating the influences of gravity and non-inertial accelerations (Flow Science, 2008).

The  $k-\varepsilon$  model, which encompasses two transport equations for turbulent kinetic energy  $k_T$  and its dissipation  $\varepsilon_T$ , represents a more intricate and widely utilized approach (Harlow, 1967). The  $k-\varepsilon$  model has demonstrated its ability to offer suitable approximations for various flow types (Rodi, 1980). In the Renormalization Group (RNG) model (Yakhot and Orszag, 1986), equations governing average turbulence quantities are obtained through statistical techniques, including those for turbulent kinetic energy and its dissipation rate. The turbulence model known as Large Eddy Simulation (LES) originated from advancements in atmospheric modeling. Its fundamental concept revolves around the notion that any turbulent flow structures that the computational grid can resolve must be identified explicitly while only approximating those aspects that are too diminutive to be directly resolved (Smith and Foster, 2005). In more detail, the four turbulence models in Flow-3D software are summarized by (Hyperinfo Corp., 2016) with pros and cons for each different model as well as tabulated in **Table 1**.

Assessment of the turbulence model is given by several research studies. Four different numerical simulation models of scouring around the bridge pier by using Flow-3D software are selected. Firstly, (Zhang, Zhou and Wang, 2017) argue that the turbulence model is a sensitive parameter in the modeling of sediment scour because it is directly affected by the viscosity as computed in Flow-3D software. The local shear stress used to measure entrainment rates and bed-load erosion rates needs to be determined by viscosity. It is suggested that the RNG  $k-\varepsilon$  model be utilized for simulating sediment scour because it significantly cuts down on computation time when compared to the Large Eddy Simulation (LES) model, which necessitates a very fine mesh. The RNG  $k-\varepsilon$  model also has a wider range of applications than the standard  $k-\varepsilon$  model, which derives some coefficients empirically and estimates others dynamically, whereas the RNG model defines all coefficients through statistical analysis. In addition, the RNG  $k-\varepsilon$  model is recognized for its ability to accurately depict low-intensity turbulence flows that exhibit stronger shear regions. Therefore, this model is employed to assess the scouring effects around the bridge pier.

Secondly, similar to the prior study, (Omara and Tawfik, 2018) employed the RNG  $k-\varepsilon$  model for simulating sediment scour through numerical methods. Accurate estimation of near-wall shear stress is crucial in sediment scouring; therefore, selecting an appropriate turbulence model for turbulent flows is essential. The RNG  $k-\varepsilon$  model is recognized for its precision in scenarios involving low-intensity turbulence and areas with intense shear. Furthermore, (Ghaderi and Abbasi, 2019) endorsed the utilization of the RNG  $k-\varepsilon$  model for simulating the average flow characteristics found in turbulent flows. They assert that even when employing a high mesh count, the RNG  $k-\varepsilon$  model can achieve reliable results. Additionally, (Jalal and Hassan, 2020) shared the same viewpoint regarding the RNG  $k-\varepsilon$  model, indicating that its applicability extends further than that of the standard  $k-\varepsilon$  model. Their research also incorporated the RNG  $k-\varepsilon$  model because: 1) it is well-suited for modeling turbulent flow around a bridge pier, 2) in terms of scouring simulation applications, the RNG  $k-\varepsilon$  model is regarded as one of the most accurate and efficient options available, 3) given the significant turbulence generated by fluid movement through control structures during scouring simulations, the RNG  $k-\varepsilon$  model exhibits superior performance.

**Table 1.** The differences in the turbulence model (Hyperinfo Corp., 2016)

Model option	Pros	Cons
Two-equation (standard k- $\epsilon$ model)	Widely used for real-world problems. Solve transport equations for turbulent kinetic energy and turbulent dissipation rate.	Valid only for fully turbulent flows, not great for high strain rates, swirling flows, or curved streamlines. Doesn't model wall heat or mass transfer well. Poor results for adverse gradients and separated flows.
Renormalized Group (RNG k- $\epsilon$ )	An improved k- $\epsilon$ model, with coefficients determined through rigorous statistical analysis. Better for transitional flows and all the other cons of the standard k- $\epsilon$ model (except swirling).	Not ideal for highly swirled flows (cyclones and shear-stress-induced secondary flows). Otherwise, usually the best choice.
Wilcox 1998 k- $\omega$ model	Similar to the standard k- $\epsilon$ model. Better near viscous boundary layer (usually not useful in big models) and better for spreading free-shear flows (jets, wakes, plumes).	More expensive than the k- $\epsilon$ model. It may not as accurate as the k- $\epsilon$ models for free-stream velocity profiles.
Large Eddy Simulation (LES)	Approaches direct numerical simulation (DNS) by directly resolving eddies larger than the computational cell scale. Applies the Smagorinsky model for eddies smaller than a cell. Contains more information than other models (e.g., magnitude and std. dev. of turbulent fluctuations).	Very computationally expensive because it requires a very fine mesh due to a simplistic model for the eddy viscosity. Interpretation of the results takes more care and knowledge than the RANS models.

### 2.2.3 Sediment scour model

The sediment scour simulation in Flow-3D considers several non-cohesive types of sediment that differ in various characteristics like grain size, density, critical shear stress, angle of repose, as well as parameters for entrainment and transport (Zhang, Zhou and Wang, 2017; Jalal and Hassan, 2020). This simulation forecasts how mixed and suspended sediments behave, encompassing processes like advection, erosion, settlement, and deposition (Flow Science, 2008) around bridge piers within a three-dimensional flow framework (Brethour, 2003). The model is applicable to various flow types, provided all sediment motions occur within a single fluid (Flow Science, 2008). It is made up of two main elements: drifting and lifting. Drifting is the process by which sediment that is carried within the flow eventually settles as a result of gravitational and other forces acting on it. The drift-flux model currently utilized in FLOW-3D relies on this concept. Lifting takes place at the boundary where packed sediment meets the fluid, specifically when the local shear stress surpasses a certain threshold. Viscosity and density are assessed as variables influenced by sediment concentration (Brethour, 2003).

The model for sediment scour comprises five key mechanisms for sediment transport: settling due to gravity, movement with the flow, scouring, bed-load transport, and deposition (Hyperinfo Corp., 2016) as shown in **Figure 2**.

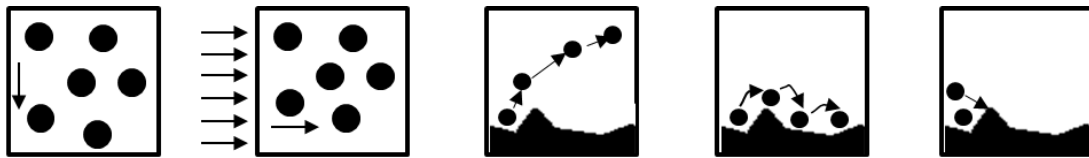


**Figure 2.** Sediment transport mechanisms (Hyperinfo Corp., 2016)

Essential factors for establishing the model consist of the important Shields number, the equation for bed-load transport rate, the highest packing fraction, the stress on the bed shear, and the properties of the sediment. The parameter known as the critical shields is linked to the essential or threshold shear stress necessary for detaching a sediment particle from the interface of a packed bed (Brethour, 2003). This relationship is influenced by the size, density, and the body forces acting on the sediment, which can lead to erosion (Flow Science, 2008). The definition of the critical shields number is categorized into two options: a prescribed value and a value that is calculated using the Soulsby-Whitehouse equation. The prescribed value indicates that the critical shields number is derived directly from Flow-3D. The other aspect, the dimensionless critical shields, is calculated through the Soulsby-Whitehouse equation (Richard Soulsby, 1997)

$$\theta_{cr,i} = \frac{0.3}{1 + 1.2d_{*,i}} + 0.055 [1 - \exp(-0.02d_{*,i})] \quad (5)$$

The movement of sediment known as bed-load transport occurs when particles roll or bounce along the surface of a consolidated sediment bed. There are three formulas established to calculate the volumetric sediment transport rate for each unit width of the bed, which include:

Meyer, Peter and Müller equation (Meyer-Peter and Müller, 1948)

$$\Phi_i = \beta_{MPM,i} (\theta_i - \theta'_{cr,i})^{1.5} c_{b,i} \quad (6)$$

Nielsen equation (Nielsen, 1992)

$$\Phi_i = \beta_{Nie,i} \theta_i^{0.5} (\theta_i - \theta'_{cr,i}) c_{b,i} \quad (7)$$

Van Rijn equation (Van Rijn, 1984)

$$\Phi_i = \beta_{VR,i} d_{*,i}^{-0.3} \left( \frac{\theta_i}{\theta'_{cr,i}} - 1.0 \right)^{2.1} c_{b,i} \quad (8)$$

Where  $\beta_{MPM,i}$ ,  $\beta_{Nie,i}$ , and  $\beta_{VR,i}$  coefficients are usually equal to 8.0, 12.0, and 0.053. By using Meyer, Peter and Müller equation, the value of bedload coefficient for low transport generally is 5.0 to 5.7, for intermediate transport is around 8.0, while for very high transport, such as sand moving in sheet flow due to waves and currents, it can reach up to 13.0. Therefore, in Flow-3D software, the standard bedload coefficient is set at 8.0 (Wei *et al.*, 2014). The variable  $c_{b,i}$  represents the volume fraction of species  $i$  found in the bed material. Although this variable is not present in the original equations, it has been included in Equations (6), (7), and (8) to consider the impact of multiple species. The symbol  $\Phi_i$  refers to the dimensionless rate of bed-load transport.

The maximum packing fraction refers to the ratio (which is the volume of all types of sediment divided by the available volume in the cell) at which the sediment in the cell is completely 'packed'. At this point, the drag function within the cell reaches infinity, indicating that there is no fluid flow occurring. This can be expressed as  $(1 - \text{porosity})$ . For uniformly randomly packed spheres, the established default maximum packing fraction is 0.64. Sand typically has a porosity that ranges from 0.3 to 0.45, which places the maximum packing fraction between 0.55 and 0.7. Bed shear stress represents the shear stress exerted on the surface of the packed bed by the fluid. It is determined using the standard wall function for three-dimensional turbulent flow, taking the wall's roughness into account.  $C_{rough}$  is a coefficient that users can define, derived from the ratio of Nikuradse roughness  $k_s$  to the median grain diameter in the packed sediment,  $d_{50}$  (Wei *et al.*, 2014). In Flow-3D, the default  $C_{rough}$  value is set at 1.0 (Flow Science, 2008), however, it is advisable to use a  $C_{rough}$  value of 2.5 (Wei *et al.*, 2014).

In the Flow-3D software, for modeling sediment scour is needed the sediment characteristics data. This includes information such as the type of sediment, the size of the sediment diameter, its mass density, the critical Shields number, the entrainment coefficient, the bedload coefficient, and the angle of repose in degrees. (Hyperinfo Corp., 2016) classifies the types of sediment complete with the following recommended data of minimum sediment size  $d_{s,i} >$ , angle of repose  $\phi_i$ , critical shields  $\theta_{cr,i}$ , and critical shear stress  $\tau_{cr}$  as shown in **Table 2**. Minimum sediment size  $d_{s,i} >$  means the smallest grain size used for modeling sediment scour in each type of sediment. The angle of repose is the steepest slope angle before grains slide by themselves. The default value of the angle of repose is  $32^\circ$  (Wei *et al.*, 2014). The critical shields parameter  $\theta_{cr,i}$  is utilized to determine the critical bed shear stress  $\tau_{cr}$ . This is the point at which sediment starts to move for both training and bedload transport.

$$\theta_{cr,i} = \frac{\tau_{cr,i}}{gd_i(\rho_i - \rho_f)} \quad (9)$$

In this context,  $g$  refers to gravity expressed as an absolute value, while  $\rho_f$  denotes the density of the fluid,  $\rho_i$  indicates the mass density of the sediment particles, and  $d_i$  represents the size of the sediment grains (Wei *et al.*, 2014). The fundamental value of  $\theta_{cr,i}$  applies to a level surface containing grains of the same size. The default value of critical shields number  $\theta_{cr,i}$  is 0.05 (Wei *et al.*, 2014) but it can also be calculated using the Soulsby-Whitehouse equation found in Eq. (5) (Richard Soulsby, 1997). When the fluid flows uphill, the critical shear stress  $\tau_{cr}$  rises, while it falls when the flow moves downhill (Wei *et al.*, 2014). For all sediment grains regardless of size have a density  $\rho_i$  equal to  $2650 \text{ kg/m}^3$ .

Entrainment refers to the action where turbulent eddies lift and keep the grains suspended from the top of the packed bed. This happens when the shear stress of the bed goes above a certain limit, known as the critical shear stress. To find the lifting velocity, which is the speed at which grains exit the packed bed, the entrainment coefficient is necessary. This coefficient can also help in measuring the scour rate. According to Wei *et al.* (2014), the standard value for the entrainment coefficient is 0.018 (Wei *et al.*, 2014).

The information of sediment scour model properties used to simulate by using Flow-3D software is given in **Table 3**. There are 4 sediments scour models are generated by some related studies in the year 2017 to 2020. Nearly all models determine the important shields number through the Soulsby-Whitehouse equation, with the exception of the Ghaderi model due to a lack of available data. For the bed-load transport rate, Zhang and Omara agreed to use the Van Rijn equation. Otherwise, the Jalal model used Meyer, Peter and Müller equation to calculate bed-load transport rate, and again there is no information

for the Gadheri model. Omara and Jalal define the value of the roughness coefficient  $C_{rough}$  as equal to 2.5 and 1.0. For the properties of the angle of repose  $\phi$  and critical shields number  $\theta_{cr}$ , the value of  $32^\circ$  and 0.05 are used by all models. Zhang and Jalal used 0.018 for entrainment coefficient in their models. However, Omara found that 0.005 gives a good result for its model. The bed-load coefficient is the final property utilized for simulating sediment scour within Flow-3D software. Zhang and Omara use the default value of 0.053 from the Van Rijn equation, then Jalal uses the value of 12 from Meyer, Peter and Müller equation after many calibrations.

**Table 2.** Sediment characteristics (Hyperinfo Corp., 2016)

Class Name (ID)	Minimum Sediment Size ( $d_{s,i} >$ )		Angle of Repose ( $\phi_i$ ) (degrees)	Critical Shields # ( $\theta_{cr,i}$ ) (dimless)	Approx. Critical Shear Stress ( $\tau_{cr}$ )		
	(inch)	(mm)			( $lb_f/ft^2$ )	(Pa)	( $g/cm^2$ )
<b>Boulder</b>							
very large	80	2048	42	0.054	37.4	1791	17907
large	40	1024	42	0.054	18.7	895	8954
medium	20	512	42	0.054	9.3	445	4453
small	10	256	42	0.054	4.7	225	2250
<b>Cobble</b>							
large	5	128	42	0.054	2.3	110	1101
small	2.5	64	41	0.052	1.1	53	527
<b>Gravel</b>							
very coarse	1.3	32	40	0.05	0.54	25.9	259
coarse	0.6	16	38	0.047	0.25	12.0	120
medium	0.3	8	36	0.044	0.12	5.7	57
fine	0.16	4	35	0.042	0.06	2.9	29
very fine	0.08	2	33	0.039	0.03	1.4	14
<b>Sand</b>							
very coarse	0.04	1	32	0.029	0.01	0.48	4.8
coarse	0.02	0.5	31	0.033	0.006	0.29	2.9
medium	0.01	0.25	30	0.048	0.004	0.19	1.9
fine	0.005	0.125	30	0.072	0.003	0.14	1.4
very fine	0.003	0.075	30	0.109	0.002	0.10	1.0
<b>Silt</b>							
coarse	0.002	0.05	30	0.165	0.001	0.05	0.48
medium	0.001	0.025	30	0.25	0.001	0.05	0.48



**Table 3.** Sediment scour model properties

Properties	Numerical research			
	(Zhang, Zhou and Wang, 2017)	(Omara and Tawfik, 2018)	(Ghaderi and Abbasi, 2019)	(Jalal and Hassan, 2020)
Critical shields number definition	Soulsby-Whitehouse eq.	Soulsby-Whitehouse eq.	*	Soulsby-Whitehouse eq.
Bed-load transport rate equation	Van Rijn eq.	Van Rijn eq.	*	Meyer, Peter and Müller eq.
Bed roughness/d50 ratio, $C_{rough}$ (dimless)	*	2.5	*	1.0
Sediment size, $d_s$ (mm)	0.85	1.8	0.56	0.385
Angle of repose, $\varphi$ (degrees)	32	32	32	32
Critical shields number, $\theta_{cr}$ (dimless)	0.05	0.05	0.05	0.05
Entrainment coefficient (dimless)	0.018	0.005	*	0.018
Bed-load coefficient (dimless)	0.053	0.053	*	12

\* data not available

### 2.2.4 Meshing

Mesh quality is critical for accurate scour modeling. Smaller mesh cell sizes lead to improved outcomes. A mesh can be defined as the grid sections that represent the variety of shapes and fluid movement (Hyperinfo Corp., 2016). In the FLOW-3D software, the orthogonal mesh is described using either cartesian or cylindrical coordinates. There are three types of mesh setups: uniform, non-uniform, and multi-block meshes. Uniform meshes have consistent cell sizes in all directions, while non-uniform meshes allow for variable cell sizes at specific locations. Intermediate points are used to identify higher resolution locations. External flows might also utilize intermediate points when a detailed view is necessary close to the area of focus, while the mesh grows larger as it moves away from the object. Multi-block meshes are used for complex geometries where single-block meshes are insufficient. Flow-3D uses the FAVOR method, which stands for Fractional Area-Volume Obstacle Representation, to reduce the staircase effect that occurs in Cartesian grids. This helps to provide a smoother representation of geometry (Flow Science, 2008).

Flow-3D employs the FAVOR method to prevent the stairstep issue that might arise from a basic cartesian grid setup. It does this by smoothly blocking fractional parts of the faces and volumes of grid cells (Flow Science, 2008). Before beginning the simulation, clicking the FAVOR button is a good way to verify that the mesh cell size is adequate. **Figure 3** shows a clear picture of the mesh cell size effect on the geometry interface, and this will influence the result accuracy. (Hyperinfo Corp., 2016) gives some recommendations for setting the mesh cell sizes. Within each mesh block, it could try to uniform cell sizes first then adjust as needed. The more cells, the longer time needed for running simulation. So, it is necessary to consider the cell size and number of cells to get an accurate result in efficient time. For single cells, the optimal outcome can be achieved with cells that have a 1:1:1 aspect ratio (x:y:z) and do not go beyond a 3:1 ratio in any two directions. For adjacent cells, the ideal result is obtained with cells having a 1:1 ratio (x:x, y:y, or z:z) and should not exceed 1.25 in the same direction (Hyperinfo Corp., 2016).

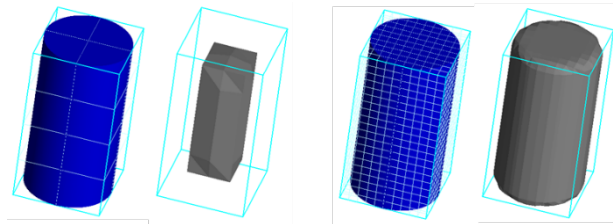


**Figure 3.** FAVORize check mesh quality for (a) cell size: 0.5 and (b) cell size: 0.1 (Hyperinfo Corp., 2016)

Some assessments were given by several studies to determine the meshing setup in sediment scour modeling using Flow-3D software. (Zhang, Zhou and Wang, 2017) argued the uniform mesh might be reduced the result accuracy. (Omara and Tawfik, 2018) emphasized that a finer mesh is necessary close to solid boundaries, such as piers and packed sediment beds, to capture flow details effectively. Significant effort has been dedicated to enhancing the computational mesh to achieve optimal grid and time convergence. A cell size of 0.003 m was implemented near the pier and sediment bed surface, gradually increasing to 0.025 m in other areas of the domain. (Ghaderi and Abbasi, 2019) employed a nested mesh approach that effectively modeled vortices while also aligning well with experimental findings. The nested mesh system consisted of an internal mesh measuring 0.022 m and an external mesh of 0.009 m, achieving a maximum aspect ratio of 1.48. It is important to maintain a similar size to the recommended ratio of the two meshes, ideally around 2, while ensuring a smooth transition in mesh size at the intersection of the two different meshes. Nevertheless, (Jalal and Hassan, 2020) suggest that using a minimum cell size of 0.005 m close to the pier will yield precise outcomes and a clear measurement of scour depth in that area, while a maximum cell size of 0.01 m would help decrease the computation duration.

### 2.2.5 Boundary conditions

Boundary conditions in Flow-3D are defined based on the geometry and specific physical models. Each mesh block has independent boundary settings, represented by capital letters. However, boundary conditions need to be determined on the faces of each mesh block by knowing the significance of each boundary condition. Flow-3D software offers a total of 10 distinct boundary conditions. One such

condition is the continuative boundary, which establishes a zero-gradient state at the edge. Another is grid overlay, utilized during restart simulations, allowing the solution from the previous simulation to serve as a boundary condition. For the outflow boundary condition, the Sommerfeld radiation state is employed to dynamically assess the conditions at the boundary. Additionally, periodic boundaries operate in pairs; any fluid that exits through one boundary will be reintroduced via the opposing boundary of the pair, with the pressure at that boundary being specified. If the fluid's elevation is defined, the boundary pressure will adhere to a hydrostatic distribution.

An additional five boundary conditions are established, including a specified velocity that determines the flow speed at the boundary. For the symmetry boundary, both a zero-gradient condition and a regular zero velocity condition are implemented. The boundary is subjected to a volume flow rate based on the established flow rate, while the wall enforces the no-slip condition along with a zero-velocity condition directed normally at the boundary. The final boundary condition pertains to the wave, which introduces a velocity field related to the requested wave type (Flow Science, 2008). The evaluation of boundary conditions in sediment scour modeling through Flow-3D software, derived from various studies, is compiled in **Table 4**. This provides an overview of how these conditions are applied from real scenarios to numerical simulations.

**Table 4.** Boundary conditions

Numerical research		(Zhang, Zhou and Wang, 2017)	(Omara and Tawfik, 2018)	(Ghaderi and Abbasi, 2019)	(Jalal and Hassan, 2020)
Boundary conditions					
X Min	Left boundary	Specified velocity	Specified velocity	Specified velocity	Specified velocity
X Max	Right boundary	Outflow	Outflow	Outflow	Outflow
Y Min	Front boundary	Symmetry	Symmetry	Wall	Symmetry
Y Max	Back boundary	Symmetry	Symmetry	Wall	Symmetry
Z Min	Bottom boundary	Wall	Wall	Wall	Wall
Z Max	Top boundary	Specified pressure	Specified pressure	Symmetry	Symmetry

Based on the data above, all studies have the same assumption for left, right, and the bottom boundary with specified velocity, outflow, and wall. For modeling the front and back boundary conditions, Zhang, Omara, and Jalal agreed to used symmetry. However, Ghaderi applied the wall as the back boundary. Then, for modeling the top boundary condition, Zhang and Omara assume specified pressure as the best model chosen. Otherwise, Ghaderi and Jalal choose symmetry as the top boundary condition.

### 3. Scouring Depth

To evaluate the accuracy of Flow-3D in simulating scour depth, numerical results from four studies were compared with experimental data and summarized as shown in Table 5 including the error rate of difference. As we can see in **Table 5**, Zhang's model achieved a 0% error rate, making it the most accurate. Other studies, such as Omara and Ghaderi, reported error rates of 0.75% and 1.75%, respectively, while Jalal's model had a 10% error rate.

**Table 5.** Scouring depth

No.	Scouring depth (m)		Error (%)	Reference
	Flow-3D results	Experimental results		
1	0.076	0.076	0%	(Zhang, Zhou and Wang, 2017) (Khosronejad, Kang and Sotiropoulos, 2012)
2	0.0397	0.040	0.75%	(Omara and Tawfik, 2018) (Ahmed and Rajaratnam, 1998)
3	0.03372	0.03432	1.75%	(Ghaderi and Abbasi, 2019) (Hasanpour N, 2012)
4	0.036	0.04	10%	(Jalal and Hassan, 2020) (Melville, 1975)

#### 4. Conclusion

This review highlights the effectiveness of Flow-3D software in simulating scour around bridge piers. There are four research studies in different years of 2017 to 2020 that have been reviewed. Flow-3D has proven to be a reliable tool to solve the sediment scour problem by defining the appropriate parameters, to accurately represent real-life situations. (Zhang, Zhou and Wang, 2017) research study is chosen as the best numerical model in simulating sediment scour depth due to the error rate between the sediment scour depth obtained by experimental and numerical simulation is 0%, that is the results of both are equal to 0,076m.

The RNG k-ε turbulence model and Soulsby-Whitehouse and Van Rijn sediment transport equations are identified as the most accurate for predicting scour depth. A finer mesh around the pier and appropriate boundary conditions further enhance model accuracy. Specified velocity and outflow are used for the left and right boundaries. Moreover, for front and back boundary were using symmetry, then the bottom and top boundary were using the wall and specified pressure. Future studies should focus on assessing scour depth evolution over time, in addition to equilibrium scour depth.

#### References

- Ahmed, F. and Rajaratnam, N. (1998) ‘Flow around Bridge Piers\_Ahmed.pdf’, *Journal of Hydraulic Engineering*, 124(March), pp. 288–300.
- Alemi, M. and Maia, R. (2016) ‘Numerical Simulation of the Flow and Local Scour Process around Single and Complex Bridge Piers’, *International Journal of Civil Engineering*, 16(5), pp. 475–487. Available at: <https://doi.org/10.1007/s40999-016-0137-8>.
- Brethour, J. (2003) ‘Modeling Sediment Scour - Flow 3D Technical Notes’, p. 6.
- Brethour, J.M. (2001) ‘Transient 3-D model for lifting, transporting, and depositing solid material’, *Proc. of the 2001 Int. Symposium on Environmental Hydraulics* [Preprint]. Available at: [http://www.flow3d.com/pdfs/tp/wat\\_env\\_tp/FloSci-Bib28-01.pdf](http://www.flow3d.com/pdfs/tp/wat_env_tp/FloSci-Bib28-01.pdf).
- Breusers, H.N.C. (1979) *Lecture Notes on Local Scour*.
- Breusers, H.N.C., Nicollet, G. and Shen, H.W. (1977) ‘Erosion locale autour des piles cylindriques’, *Journal of Hydraulic Research*, 15(3), pp. 211–252. Available at: <https://doi.org/10.1080/00221687709499645>.

Briaud, J.-L., Gardoni, P. and Yao, C. (2012) 'Bridge Scour Risk', *Proceedings of the 6th International Conference on Scour and Erosion*, pp. 1193–1210.

Flow Science (2008) *Flow-3D User Manual Version 9.3*. Available at: [www.flow3d.com](http://www.flow3d.com).

Ghaderi, A. and Abbasi, S. (2019) 'CFD simulation of local scouring around airfoil-shaped bridge piers with and without collar', *Sadhana - Academy Proceedings in Engineering Sciences*, 44(10), p. 216. Available at: <https://doi.org/10.1007/s12046-019-1196-8>.

Ghasemi, M. and Soltani-Gerdefaramarzi, S. (2017) 'The Scour Bridge Simulation around a Cylindrical Pier Using Flow-3D', *Journal of Hydrosiences and Environment*, 1(2), pp. 46–54. Available at: <https://doi.org/10.22111/jhe.2017.3357>.

Hamill, L. (Leslie) (1999) *Bridge hydraulics*. London: E. & FN Spon.

Harlow, F.H. (1967) 'Turbulence Transport Equations', *Physics of Fluids*, 10(11), p. 2323. Available at: <https://doi.org/10.1063/1.1762039>.

Hasanpour N, H.D.A. and A.H. (2012) 'Investigation of Local Scour around Airfoil Shaped Pier with Collar', *Sci. Soil and Water*, 23(3), pp. 221–234.

Hyperinfo Corp. (2016) *Flow-3D v11.2*. Taiwan.

Jalal, H.K. and Hassan, W.H. (2020) 'Three-dimensional numerical simulation of local scour around circular bridge pier using Flow-3D software', *IOP Conference Series: Materials Science and Engineering*, 745(1). Available at: <https://doi.org/10.1088/1757-899X/745/1/012150>.

Khosronejad, A., Kang, S. and Sotiropoulos, F. (2012) 'Experimental and computational investigation of local scour around bridge piers', *Advances in Water Resources*, 37, pp. 73–85. Available at: <https://doi.org/10.1016/j.advwatres.2011.09.013>.

Melville, B.W. (1975) *Local scour at bridge sites*. University of Auckland.

Meyer-Peter, E. and Müller, R. (1948) 'Formulas for Bed-Load Transport', *Proceedings of the 2nd Meeting of the International Association of Hydraulic Research*, pp. 39–64.

Nielsen, P. (1992) *Coastal bottom boundary layers and sediment transport*. Advanced s. Singapore: World Scientific Publishing.

Omara, H. and Tawfik, A. (2018) 'Numerical study of local scour around bridge piers', *IOP Conf. Series: Earth and Environmental Science*, 151. Available at: <https://doi.org/10.1088/1755-1315/151/1/012013>.

Prendergast, L.J. and Gavin, K. (2014) 'A review of bridge scour monitoring techniques', *Journal of Rock Mechanics and Geotechnical Engineering*, 6(2), pp. 138–149. Available at: <https://doi.org/10.1016/j.jrmge.2014.01.007>.

Richard Soulsby (1997) *Dynamics of marine sands*. Ch 9. London: Thomas Telford Publications.

Richardson, J.E. and Panchang, V.G. (1998) 'Three-Dimensional Simulation of Scour-Inducing Flow at Bridge Piers', *Journal of Hydraulic Engineering*, 124(5), pp. 530–540. Available at: [https://doi.org/10.1061/\(asce\)0733-9429\(1998\)124:5\(530\)](https://doi.org/10.1061/(asce)0733-9429(1998)124:5(530)).

Van Rijn, L.C. (1984) 'Sediment transport, Part I: bed load transport', *Journal of Hydraulic Engineering*, 110, pp. 1431–1456. Available at: [https://doi.org/10.1061/\(ASCE\)0733-9429\(1984\)110:10\(1431\)](https://doi.org/10.1061/(ASCE)0733-9429(1984)110:10(1431)).

Rodi, W. (1980) *Turbulence models and their application in hydraulics – A state of the art review*. Netherlands: International. Association for Hydraulic Research, Delft.

Smith, H.D. and Foster, D.L. (2005) ‘Modeling of Flow Around a Cylinder Over a Scoured Bed’, *Journal of Waterway, Port, Coastal, and Ocean Engineering*, 131(1), pp. 14–24. Available at: [https://doi.org/10.1061/\(asce\)0733-950x\(2005\)131:1\(14\)](https://doi.org/10.1061/(asce)0733-950x(2005)131:1(14)).

Soltani-Gerdefamarzi, S., Afzalimehr, H., Chiew, Y.M., *et al.* (2013) ‘Jets to control scour around circular bridge piers’, *Canadian Journal of Civil Engineering*, 40(3), pp. 204–212. Available at: <https://doi.org/10.1139/cjce-2012-0240>.

Soltani-Gerdefamarzi, S., Afzalimehr, H., Yee-Meng Chiew, J.G., *et al.* (2013) ‘Turbulent Characteristics in Flow Subjected to Bed Suction and Jet Injection as a Pier-Scour Countermeasure’, *International Journal of Hydraulic Engineering*, 2(5), pp. 93–100.

Wang, C., Liang, F. and Yu, X. (2016) ‘Experimental and numerical investigations on the performance of sacrificial piles in reducing local scour around pile groups’, *Natural Hazards*, 85(3), pp. 1417–1435. Available at: <https://doi.org/10.1007/s11069-016-2634-0>.

Wei, G. *et al.* (2014) ‘The Sediment Scour Model in FLOW-3D’, FSI-14-TN9(June), pp. 1–26.

Yakhot, V. and Orszag, S.A. (1986) ‘Renormalization group analysis of turbulence. I. Basic theory’, *Journal of Scientific Computing*, 1(1), pp. 3–51. Available at: <https://doi.org/10.1007/BF01061452>.

Zhang, Q., Zhou, X.L. and Wang, J.H. (2017) ‘Numerical investigation of local scour around three adjacent piles with different arrangements under current’, *Ocean Engineering*, 142(July), pp. 625–638. Available at: <https://doi.org/10.1016/j.oceaneng.2017.07.045>.